IEEE Access
Multidisciplinary : Rapid Review : Open Access Journal

Received January 27, 2021, accepted April 9, 2021, date of publication April 15, 2021, date of current version May 6, 2021.

Digital Object Identifier 10.1109/ACCESS.2021.3073364

Constant Speed Control of Slider-Crank Mechanisms: A Joint-Task Space Hybrid Control Approach

JUAN ALEJANDRO FLORES-CAMPOS[1], (Member, IEEE), ADOLFO PERRUSQUÍA[2], (Member, IEEE), LUIS HÉCTOR HERNÁNDEZ-GÓMEZ[3], NOÉ GONZÁLEZ[3], AND ALEJANDRA ARMENTA-MOLINA[3]

[1]Unidad Profesional Interdisciplinaria en Ingeniería y Tecnologías Avanzadas, Instituto Politécnico Nacional (UPIITA-IPN), Ciudad de México 07340, México
[2]School of Aerospace, Transport and Manufacturing, Cranfield University, Bedford MK43 0AL, U.K.
[3]Instituto Politécnico Nacional, ESIME Unidad Zacatenco, Sección de Estudios de Posgrado e Investigación, Unidad Profesional Adolfo López Mateos, Ciudad de México 07738, México

Corresponding author: Juan Alejandro Flores-Campos (jaflores@ipn.mx)

This work was supported by Secretaría de Investigación y Posgrado, Instituto Politécnico Nacional (SIP-IPN) under Project SIP: 20210932 and Project SIP: 20210512.

ABSTRACT In this paper, a constant speed control of slider-crank mechanisms for machine tools is proposed. A joint-task space hybrid controller based on a second-order sliding mode control and time-base generator was used to guarantee a constant speed trajectory tracking and a complete turn of the mechanism crank. A switching criterion was implemented in order to avoid the singularities located at the two extreme positions of the slider stroke. A trapezoidal speed profile with parabolic blends was designed directly over task space slider trajectory considering a constant cutting speed, the workpiece dimensions and the slider stroke length. Stability of the second-order sliding mode control was validated with the Lyapunov stability theory. Simulations were carried out to verify this approach.

INDEX TERMS Slider-crank mechanism, singularity points, sliding mode control, time-based generator, constant cutting speed, switching criterion.

I. INTRODUCTION

The slider-crank mechanism is also known as quick-return mechanism. It is a closed-chain mechanism and is widely used in machines and cutting tools. The dynamic instability of the cutting process is reduced. Besides, high cutting speeds with higher contact forces can be obtained at low cost [1]. Its main stroke is slow, while the return stroke is fast. It is commonly used in shapers, motorized saws, bombs, among others [2].

The output-link is controlled indirectly by means of the input-crank in joint-space [2], [3]. Although, the control task is performed by the output link (slider) in task space. Joint space control does not deal with the singularity points at the beginning and the end of the slider stroke [4]. The joint space controller can take advantage of the mechanical advantage[1] of the mechanism without losing controllability [5] and ensuring a complete turn of the mechanism crank.

The associate editor coordinating the review of this manuscript and approving it for publication was Bo Shen.

[1]The mechanical advantage is a measure of the output force amplification.

The movement of the slider is linear due to the mechanism configuration [6]. So, it is advisable to control the mechanism in task space. For cutting tasks, the slider has contact with the workpiece (usually the workpiece is modeled as a spring system or a spring-damper system [7]). This contact generates an external force in the opposite direction to the slider movement, which can be seen as a perturbation [8]–[10]. Since this perturbation occurs in task space, it requires that the Jacobian component of the slider maps the contact force from task space to joint space with the virtual work principle.

The main problem of the Jacobian is that it is equal to zero at the singularity points. Therefore, the complete turn of the input crank cannot be guaranteed; in consequence, the mechanism mechanical advantage is not used [11]. In order to avoid the Jacobian, it is proposed the use of robust joint space controllers [12]–[14], such as sliding mode control. In this case, the perturbation is compensated [15]–[17]. Although task space controllers can deal more properly with the slider position control, they are avoided due to the presence of singularities [18], [19].

This work is licensed under a Creative Commons Attribution 4.0 License. For more information, see https://creativecommons.org/licenses/by/4.0/

A common objective of the slider-crank mechanisms in manufacture applications is to achieve a constant cutting speed at the slider link, $\dot{x} = v$, in order to get uniform cuts throughout the workpiece [20], [21]. Here v denotes a constant cutting speed which determines the final surface roughness of the machined workpiece [20].

This problem has a wide interest and there are several approaches to solve it. Classical approaches use the reciprocating method [22], [23] where a constant angular velocity, $\dot{q} = \omega$, is applied at the input link such as an approximate constant linear velocity, $\dot{x} \approx v$, is generated at the output link. However, it depends on the mechanism geometric configuration. Some authors use mechanism synthesis [9], [24] in the reciprocating method. This approach uses some relevant points of the desired trajectory in order to determine the kinematic parameters and the mechanism configuration; then a constant speed of the output link is obtained. The solution of the synthesis method is a fixed configuration of the mechanism. It has an inherent structural error which causes low versatility. In addition, the range of the cutting velocities is reduced.

In [25], flexibility of the output motion is obtained by the variation of the input-speed. The desired output motion is obtained by varying the crank speed. However, a kinematic analysis and an optimization are required [2], [3], [26], [27] for the design of an adequate trajectory. The approach also fails to consider singularities of slider stroke, contact force and the mechanical advantage in the analysis [28]. The solution of this method has a fixed mechanism configuration and an approximate constant velocity profile is obtained by the control of both, the cutting and return stroke.

In summary, the areas of opportunity or problems to be exploited in this work are:

- **a.** The reciprocating method is in joint space and does not guarantee a constant cutting velocity at the cutting tool .
- **b.** The final output of a mechanism synthesis procedure is a fixed mechanism configuration with low versatility.
- **c.** The above approaches do not consider the type of material, length, cutting forces and velocities.
- **d.** The mechanical advantage of the return stroke is not exploited.

In this paper, a constant speed control of slider-crank mechanism which addresses the above areas of opportunity is obtained, in order to generate uniform cuts throughout the workpiece by means of an hybrid joint-task space controller. Figure 1 shows the closed-loop diagram of the proposed approach. This approach integrates some geometric properties of slider-crank mechanisms in the task-space control design. The cutting stroke is controlled by a task space controller based on a second-order sliding mode controller and a time-based generator (TBG). The return stroke is controlled in open-loop by a constant joint space torque $\tau = T$, $T \in \mathbb{R}$. In order to avoid the singularity points and ensure a complete turn of the input crank, a switching criterion is proposed which switches the task space controller into the open loop joint space controller and vice versa. The switching criterion is applied in two points which are near to the singularity points. Numerical simulations have been carried out to verify our approach using a Whitworth mechanism.

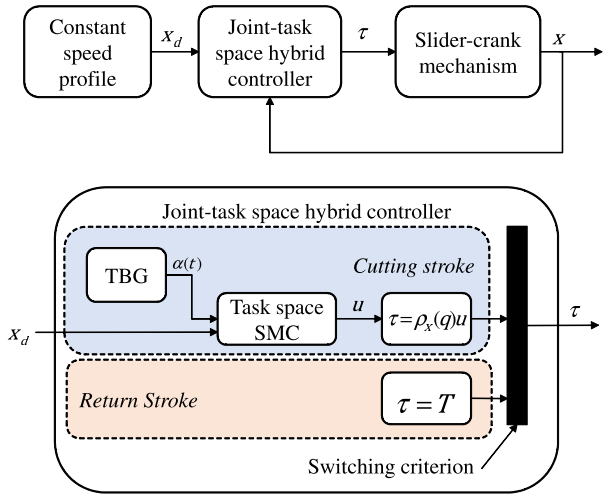

FIGURE 1. Closed-loop system diagram of the proposed approach.

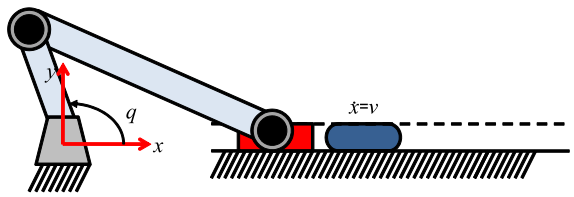

FIGURE 2. Slider-crank mechanism considered in the development of the constant speed control.

The contributions of this work are:

1) The cutting stroke is controlled in closed-loop and ensures a constant cutting speed. Meanwhile, the return stroke is controlled in open-loop by a constant torque (Solution of problems **a.** and **d.**).
2) The proposed approach can be applied to any slider-crank mechanism (Solution of problem **b.**).
3) The velocity profile is designed in accordance with the slider stroke and workpiece (Solution of problem **c.**).
4) The complete turn of the crank is guaranteed and the Jacobian singularities are avoided using the proposed switching criterion (Solution of problems **a.** and **d.**).

The outline of the paper is as follows: Section II is related with the statement of the problem, Section III shows the switching criterion for the singularity points avoidance; the speed profile design is proposed in Section IV and the controller design is shown in Section V; the simulation studies are discussed in Section VI, and Section VII concludes the paper.

II. STATEMENT OF THE PROBLEM

Consider the classical slider-crank mechanism illustrated in Figure 2. The red block is the slider or cutting tool and the blue block is the workpiece to be machined.

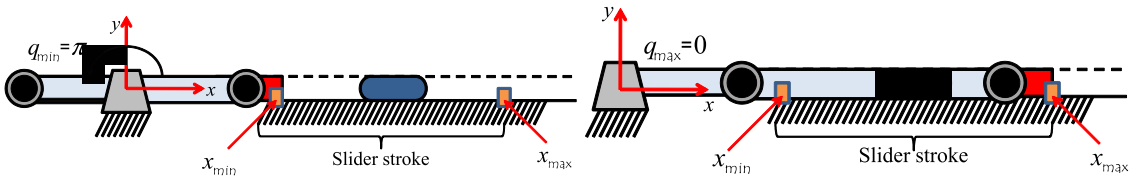

(a) Singularity at the beginning of the slider stroke.

(b) Singularity at the end of the slider stroke.

FIGURE 3. Singularity problems of a slider-crank mechanism.

The operation of slider-crank mechanisms is divided into two strokes: (1) cutting stroke and (2) return stroke. The first one is slow and it has a high mechanical advantage. On the other hand, the return stroke is fast and does not perform any operation. The main goal of this paper is to ensure a constant cutting speed, $\dot{x} = v$, of the slider. In this way, uniform cuts at the workpiece can be obtained. Accordingly, the cutting stroke is controlled. It is directly related with the mechanism natural function.

In this paper, a hybrid joint-task space controller for slider-crank mechanisms is proposed. The task-space controller generates a constant speed during the cutting stroke. Meanwhile, the return stroke is controlled in open-loop using a constant torque in joint-space.

One of the main problems of task space controllers are the singularities. Two of them are well identified for any slider-crank mechanism. They are located at the beginning and at the end of the slider stroke (see Figure 3). $x_{\min}$ and $x_{\max}$ are the singularity points at the beginning and end of the slider stroke, respectively; $q_{\min}$ and $q_{\max}$ are the inverse kinematics solution of $x_{\min}$ and $x_{\max}$. Besides, the points $x_{\min}$ and $x_{\max}$ define the transitions from the cutting stroke to the return stroke and vice versa. Since the cutting stroke is controlled by a task-space controller, then the use of the Jacobian $\rho_x(q)$ is mandatory. Nevertheless, the Jacobian is equal to zero at the singularity points, i.e., $\rho_x(q_{\min}) = \rho_x(q_{\max}) = 0$.

In this paper, it is proposed a switching criterion which shifts the task-space controller to the joint space controller and vice versa. In this way, a complete turn of the mechanism crank takes place.

III. SWITCHING CRITERION DESIGN

Regarding the first contribution, the phase diagram of the slider link, shown in Figure 4, was considered. The slider link is controlled by a joint space controller using the reciprocating method, i.e., a constant angular velocity at the input crank was supposed such as the slider presents an approximate constant linear speed.

The phase diagram shows that the cutting stroke and the return stroke are controlled by the joint space controller. The singularity points do not affect the closed-loop performance. However, this approach does not take advantage of the mechanical advantage during the return stroke. Also, there is no sense to control the return stroke because any operation is developed. There is a small interval during the

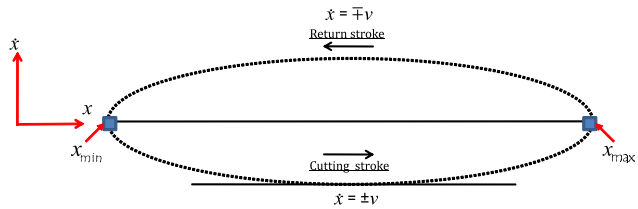

FIGURE 4. Phase diagram of the output link in a joint space control scheme.

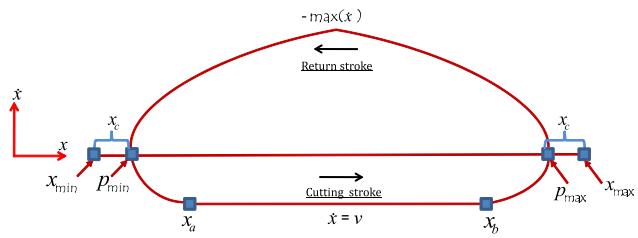

FIGURE 5. Phase diagram of the output link. Task space control.

cutting stroke, in which the cutting speed is approximately constant.In this case, the length of the workpiece is not considered. As a result, this approach cannot ensure uniform cuts throughout the workpiece and it affects the final roughness. Furthermore, the slider velocity is not constant in most cases, since it depends on the geometric configuration of the mechanism.

To the best of our knowledge, task-space controllers have not been widely studied in the design of a constant speed control of slider-crank mechanisms because the controllability at the singularity points is lost [29].

In order to avoid the singularity points at the ends of the cutting stroke, a switching criterion has been proposed. It modifies the operation mode of the controller before the mechanism arrives at a singularity point, as it is shown in Figure 5.

At this respect, four new points, $p_{\min}$, $p_{\max}$, x_a and x_b have been defined. The points $p_{\min}$ and $p_{\max}$ are the left and right switching limit points, respectively. They are located before the singularity points at a constant threshold distance x_c. The range of the possible values for the threshold x_c should be based on a prior analysis of the dynamic performance of the mechanism. At the same time, the following restrictions are satisfied: $x_c \in (x_{\min}, p_{\min})$ and $x_c \in (p_{\max}, x_{\max})$. The points x_a and x_b are the ends of the workpiece and the center of the

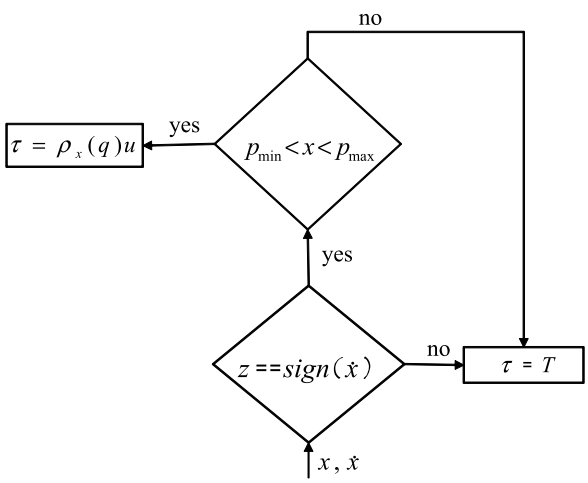

FIGURE 6. Switching criterion scheme. The diagram is read from bottom to top.

workpiece matches with the mean position of the complete slider stroke.

The switching limit points $p_{\max}$ and $p_{\min}$ are obtained by the following expressions

$$p_{\max} = x_{\max} - x_c \tag{1}$$

$$p_{\min} = x_{\min} + x_c \tag{2}$$

Therefore, the switching criterion is defined as

$$p_{\min} < x < p_{\max} \tag{3}$$

The switching criterion (3) consists of the following *if-else* condition: if the slider position x is between $p_{\min}$ and $p_{\max}$, then the task-space controller, which will be discussed in the future sections, is applied. On the other hand, if (3) is not satisfied, then a constant torque is applied, $\tau = T$ (T is a constant torque value), to return the mechanism to the left switching point $p_{\min}$ and start over the cutting stroke.

The main problem of this criterion is to identify when the mechanism is at the cutting or return stroke. A useful quality of slider-crank mechanisms is that the direction of the slider speed at the cutting and return strokes is opposite to the displacement. Therefore, it is proposed to use the sign of the slider speed (see Figure 6) to determine which stroke the mechanism is taken place. The sign can be obtained off-line by looking to the slider speed at any stroke [30].

Let z be the sign of the slider speed at the cutting stroke. Consider that $z = -1$ and the mechanism position satisfies the switching limits (3), then if the sign of the current slider speed is positive, $\text{sign}(\dot{x}) = +1$, the switching criterion applies a constant torque to return the mechanism to the switching point $p_{\min}$. On the other hand, if $\text{sign}(\dot{x}) = -1$ then the mechanism is in the cutting stroke and the switching criterion applies the task space controller.

During the return stroke, the switching criterion applies a constant torque to drive the slider mechanism to the switching limit point $p_{\min}$. Nevertheless, this is not true because the constant torque drives the mechanism to the singularity point

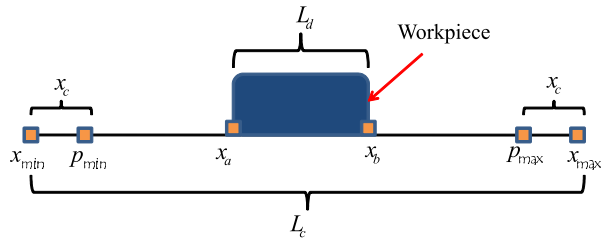

FIGURE 7. Parameters of the Speed profile in terms of the workpiece and slider stroke lengths.

$x_{\min}$, since the return stroke is not controlled. So, it is required to modify the return stroke trajectory, in such a way that it converges to $p_{\min}$, instead of $x_{\min}$. This problem is solved by using a TBG approach, which is discussed in the following sections.

IV. CONSTANT SPEED PROFILE

In this section, a constant speed profile is discussed. It is based on the phase diagram of Figure 5. For this purpose, the points x_a, x_b, $x_{\min}$, $x_{\max}$, $p_{\min}$ and $p_{\max}$ are obtained in terms of the length of the workpiece, the desired constant cutting speed v and the slider stroke length. Figure 7 shows the main parameters of the speed profile in terms of the workpiece and slider stroke lengths.

The workpiece length is denoted by $L_d = x_b - x_a$ and $L_c = x_{\max} - x_{\min}$ is the length of the slider stroke. In this paper, a trapezoidal profile with parabolic blends has been proposed. It has a smooth transient performance between the switching points ($p_{\min}, p_{\max}$) and the workpiece ends (x_a, x_b). Besides it makes easier the constant cutting speed trajectory design.

Let t_a be the time of the trapezoidal trajectory from $p_{\min}$ to x_a; t_c denotes the machining time from x_a to x_b; and t_d be the time from x_b to $p_{\max}$. In most cases, the user must provide an initial time t_0 and a final time t_f, in order to design the desired trajectory. However, the time t_f is unknown on these kind of applications because it depends on the constant cutting speed v and the length of the workpiece L_d. Therefore, it is proposed to use a wide interval of time, t_a and t_d, in such a way that the proposed trapezoidal trajectory is almost symmetric.

In accordance with the schemes shown in Figures 5 and 7, the times t_a, t_c and t_d can be calculated as

$$\begin{aligned} t_c &= \frac{L_d}{|v|} \\ t_a &= t_d = \frac{L_c}{|v|}. \end{aligned} \tag{4}$$

As a result of the symmetry $t_a = t_d$. The ends of the piece x_a and x_b are obtained in the following way

$$x_a = p_{\min} + \tfrac{v}{2t_a} t_a^2 \tag{5}$$

$$x_b = p_{\min} + \tfrac{v}{2t_a} t_a^2 + v t_c \tag{6}$$

Algorithm 1 shows the steps to calculate the parameters of the proposed constant speed profile.

Algorithm 1 Determination of the Speed Profile Parameters

Require: Tolerance threshold x_c, length of the workpiece L_d, length of the slider stroke L_c, desired constant velocity v, and the forward and inverse kinematics solutions of the slider-crank mechanism.

1: The joint positions $q_{\max}$ and $q_{\min}$, where the Jacobian is singular, i.e., $\rho_x(q_{\max}) = 0$ and $\rho_x(q_{\min}) = 0$, are obtained using the inverse kinematics solution.
2: Forward kinematics is used to obtain $x_{\min}$ and $x_{\max}$ with $q_{\min}$ and $q_{\max}$, respectively.
3: The switching limit points $p_{\max}$ and $p_{\min}$ are calculated with (1) and (2).
4: The trajectory times are calculated with (4).
5: The ends of the workpiece x_a and x_b are obtained with (5) and (6).

Ensure: $x_{\max}, x_{\min}, x_a, x_b, p_{\max}, p_{\min}, t_a, t_d$.

The proposed trapezoidal profile $x_d \in C^2 \subset \mathbb{R}^m$ is designed with the following restrictions

$$t_0 \leq t < (t_0 + t_a) \begin{cases} x_d = p_{\min} + \dfrac{v}{2t_a}(t - t_0)^2 \\ \dot{x}_d = \dfrac{v}{t_a}(t - t_0) \\ \ddot{x}_d = \dfrac{v}{t_a} \end{cases} \tag{7}$$

$$A \leq t < B \begin{cases} x_d = p_{\min} + \dfrac{vt_a}{2} + v(t - t_0 - t_a) \\ \dot{x}_d = v \\ \ddot{x}_d = 0 \end{cases} \tag{8}$$

where $A = t_0 + t_a$ and $B = t_0 + t_a + t_c$.

$$C \leq t < D \begin{cases} x_d = p_{\min} + \dfrac{vt_a}{2} + vt_c - \dfrac{v}{2t_d}(E^2 - t_d^2) \\ \dot{x}_d = -\dfrac{v}{t_d}E \\ \ddot{x}_d = -\dfrac{v}{t_d} \end{cases} \tag{9}$$

where $C = B$, $D = B + t_d = t_0 + t_a + t_c + t_d$ and $E = t - t_0 - t_a - t_c - t_d$.

$$t < t_0 \begin{cases} x_d = p_{\min} \\ \dot{x}_d = 0 \\ \ddot{x}_d = 0 \end{cases} \tag{10}$$

$$t \geq D \begin{cases} x_d = p_{\min} + (2t_c + t_a + t_d)\dfrac{v}{2} \\ \dot{x}_d = 0 \\ \ddot{x}_d = 0 \end{cases} \tag{11}$$

V. CONTROLLER DESIGN

A first order sliding mode control (SMC) has been proposed. It guarantees a robust trajectory tracking in finite time. The SMC is based on a time base generator (TBG) which attracts the return stroke trajectory and forces the convergence to $p_{\min}$.

A. SLIDER LINEAR DYNAMICS

Firstly, the slider dynamic model is discussed. Based on the Euler-Lagrange formulation [31], the extended dynamic model of a 1-DOF slider-crank mechanism with an external contact force is

$$\begin{aligned} \boldsymbol{M}'(\boldsymbol{q}')\ddot{\boldsymbol{q}}' + \boldsymbol{C}'(\boldsymbol{q}', \dot{\boldsymbol{q}}')\dot{\boldsymbol{q}}' + \boldsymbol{G}'(\boldsymbol{q}') \\ = \boldsymbol{\rho}^{-\top}(\boldsymbol{q}')\tau - \boldsymbol{\rho}^{-\top}(\boldsymbol{q}')\rho_x(\boldsymbol{q}')F_x, \end{aligned} \tag{12}$$

where $\boldsymbol{q}' = [q, \boldsymbol{s}]^\top \in \mathbb{R}^{n'}$ are the extended coordinates whose components are the generalized coordinate q and all the n secondary variables $\boldsymbol{s} \in \mathbb{R}^n$. $\boldsymbol{M}'(\boldsymbol{q}') \in \mathbb{R}^{n' \times n'}$ denotes a symmetric positive definite inertia matrix, $\boldsymbol{C}'(\boldsymbol{q}', \dot{\boldsymbol{q}}') \in \mathbb{R}^{n' \times n'}$ stands for the centrifugal and Coriolis matrix, $\boldsymbol{G}'(\boldsymbol{q}') \in \mathbb{R}^{n'}$ is the gravity vector, $\boldsymbol{\rho}(\boldsymbol{q}') \in \mathbb{R}^{n'}$ is the Jacobian vector in terms of $\boldsymbol{q}'$, $\rho_x(\boldsymbol{q}')$ is the Jacobian component that gives the mapping between the joint velocity $\dot{q}$ and the slider velocity $\dot{x}$, F_x is the slider contact force and $\tau \in \mathbb{R}$ is the control input.

It has been shown in [32] that the slider dynamics can be expressed as a linear system with a disturbance as

$$m\ddot{x} + G = \left(\sum_{i=1}^{n'} \rho_i^2(\boldsymbol{q}')\right)^{-1} \rho_x(\boldsymbol{q}')(\tau - \rho_x(\boldsymbol{q}')F_x). \tag{13}$$

where m is the slider mass, G models the slider gravity force component that depends on the mechanism configuration. The dynamics (13) can be rewritten as

$$\ddot{x} = bu + d \tag{14}$$

where $b = 1/m$ and

$$u = \left(\sum_{i=1}^{n'} \rho_i^2(\boldsymbol{q}')\right)^{-1} \rho_x(\boldsymbol{q}')\tau$$

$$d = -\frac{1}{m}\left[G + \left(\sum_{i=1}^{n'} \rho_i^2(\boldsymbol{q}')\right)^{-1} \rho_x^2(\boldsymbol{q}')F_x\right].$$

The control input u is in task space and it has to be transformed into the driven torque for real-time applications as

$$\tau = \rho_x(\boldsymbol{q}')u \tag{15}$$

B. TIME BASE GENERATOR

Consider the following sliding surface manifold,

$$s(t) = \alpha(t)e + \dot{e}, \tag{16}$$

where $e = x_d - x$, $\dot{e} = \dot{x}_d - \dot{x}$ are the position error and the velocity error in task space, respectively and

$$\alpha(t) = \alpha_0 \frac{\dot{\xi}}{(1 - \xi) + \delta} \tag{17}$$

it is a time variable gain, with $\alpha_0 = 1 + \varepsilon$, $0 < \varepsilon \ll 1$, and $0 < \delta \ll 1$. The TBG, $\xi(t) \in C^2$, is a terminal attractor [15]. The user must provide it, in such a way that ξ goes smoothly from 0 to 1 in a finite time $t = t_b > 0$. $\dot{\xi}$ is a bell shaped function, such that $\dot{\xi}(t_0) = \dot{\xi}(t_b) = 0$ with a maximum value

in $t = 0.5t_b$ and $\ddot{\xi}(0.5t_b) = 0$ at the switching hyperplane $s = 0$. So (16) is rewritten as

$$\dot{e} = -\alpha(t)e. \tag{18}$$

The solution of (18) is

$$e(t) = e(t_0)\left((1-\xi)+\delta\right)^{\alpha_0}. \tag{19}$$

Keep in mind that t_b is independent of any initial condition, therefore

$$\xi(t_b) = 1 \implies e(t_b) = e(t_0)\delta^{\alpha_0} > 0 \tag{20}$$

can be made arbitrarily small in an arbitrary finite time t_b. One way to compute ξ is by means of a 5th order spline [33] as

$$\xi(t) = 10\frac{(t-t_0)^3}{(t_b-t_0)^3} - 15\frac{(t-t_0)^4}{(t_b-t_0)^4} + 6\frac{(t-t_0)^5}{(t_b-t_0)^5} \tag{21}$$

Note that t_b defines the desired time where the mechanism trajectory of the return stroke converges to the switching point $p_{\min}$. Furthermore, the TBG initializes the controller at the surface manifold in finite time. In this paper, the time t_b is obtained empirically as follows

$$t_b = t_0 + \frac{4t_a}{5}. \tag{22}$$

C. SLIDING-MODE CONTROL

The proposed second-order SMC is [34]

$$u = k_1(\alpha(t)e + \dot{e} + k_2k_x), \quad k_1, k_2 > 0 \tag{23}$$

$$\dot{k}_x = \text{sign}(\sigma) \tag{24}$$

$$\sigma = s(t) - s(t_0)\exp^{-\lambda(t-t_0)}, \quad \lambda > 0. \tag{25}$$

$$s_x = \sigma + k_2k_x \tag{26}$$

The dynamics (24) overcomes the chattering effect of the SMC. The second term in (25) ensures that the SMC always starts on the sliding manifold. The closed-loop error dynamics between the slider dynamics (14) under the trapezoidal trajectory (7)-(11) and control (23) is

$$\ddot{e} = \ddot{x}_d - bk_1\left(\alpha(t)e + \dot{e} + k_2\int_{t_0}^{t}\text{sign}(\sigma)d\varsigma\right) - d. \tag{27}$$

The following theorem establishes the stability and boundedness of the closed-loop error dynamics.

Theorem 1: Consider the error dynamics (27) among the slider dynamics (14), the trapezoidal trajectory (7)-(11) and the sliding mode controller (23). Then, the trajectories of (27) are ultimate uniformly bounded (UUB) if the sliding gain satisfies

$$k_1 > \frac{\bar{\eta}}{b} + k_0 \tag{28}$$

where $\bar{\eta}$ is the upper bound of the perturbation and $k_0 > 0$. Furthermore, the tracking error e converges into a small ball of radius $\mu = e(t_0)\delta^{\alpha_0}$ as $t \to t_b$ and hence $\dot{e} \to 0$.

Proof: Consider the following Lyapunov function

$$V(s_x) = \frac{1}{2}s_x^2 \tag{29}$$

The time derivative of V is:

$$\begin{aligned}\dot{V}(s_x) &= s_x\dot{s}_x \\ &= s_x(\alpha(t)\dot{e} + \dot{\alpha}(t)e + \lambda s(t_0)\exp^{-\lambda(t-t_0)} + \ddot{e})\end{aligned}$$

Substituting (27) into $\dot{V}$ yields:

$$\dot{V} = s_x(\alpha\dot{e} + \dot{\alpha}e + \lambda s(t_0)\exp^{-\lambda(t-t_0)} + \ddot{x}_d - bk_1s_x - d)$$

Note that $\alpha(t)$ and its time derivative are bounded because ξ and $\dot{\xi}$ are bounded signals. The terms $|d| \leq \bar{d}$, $|\lambda s(t_0)\exp^{-\lambda(t-t_0)}| \leq \lambda|s(t_0)|$ and $|\ddot{x}_d|$ are bounded too. Defining

$$|\alpha(t)||\dot{e}| + |\dot{\alpha}(t)||e| + \lambda|s(t_0)| + |\ddot{x}_d| + \bar{d} \leq \eta(t) \tag{30}$$

where $\eta(t)$ is a state-dependent function. The time derivative $\dot{V}$ reduces to

$$\begin{aligned}\dot{V} &\leq -bk_1s_x^2 + s_x\eta(t)) \\ &\leq -|s_x|\left(bk_1|s_x| - \bar{\eta}\right)\end{aligned} \tag{31}$$

if k_1 is chosen such that it satisfies (28) then

$$|s_x| > \frac{\bar{\eta}}{bk_1} \equiv \epsilon. \tag{32}$$

The time derivative of $\dot{V}$ is negative definite and s_x converges to a bounded set S_ϵ of radius ϵ centered in $s_x = 0$ as $t \to \infty$, i.e., $s_x \leq \epsilon$.

The following is a consequence of the result discussed above

$$\sigma = s(t) - s(t_0)\exp^{-\lambda(t-t_0)} = 0$$

When time increases, the second term in σ fades and the manifold only depends on $s(t)$. Then

$$\sigma = s(t) = \alpha(t)e + \dot{e} = 0.$$

Its solution is given in (19) as

$$e(t) = e(t_0)\left((1-\xi)+\delta\right)^{\alpha_0}.$$

It means that the error is bounded in a small ball of radius $\mu = e(t_0)\delta^{\alpha_0}$ which can be arbitrarily small. This completes the proof. ■

The switching criterion, the trapezoidal velocity profile, the SMC and the TBG are the elements that constitute the complete solution, which has been proposed. It can be applied to any slider-crank mechanism.

D. TEMPERATURES IN CUTTING TASKS

The heat and temperature generated between the workpiece and the slider (cutting tool) has to be taken into account. Such heat is generated by the plastic deformation energy that transforms itself into heat. The heat generation rate, Q (W), is given by [35]

$$Q = 1.68af^{0.15}v^{0.85} \tag{33}$$

where a is the depth of the cut, f is the feed rate and v is the cutting speed. The cutting temperature is given by [36]

$$\Theta = v^{0.5}f^{0.3} \tag{34}$$

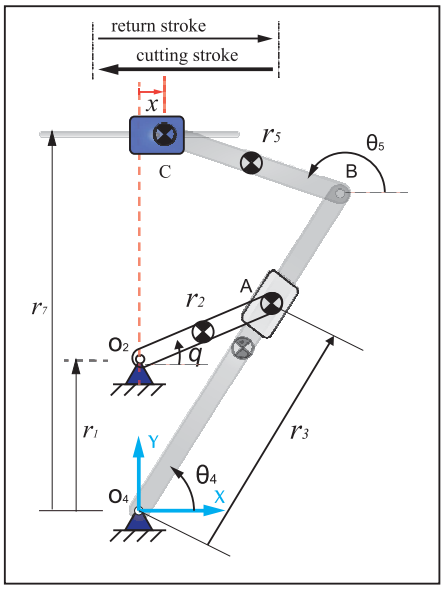

FIGURE 8. Whitworth mechanism.

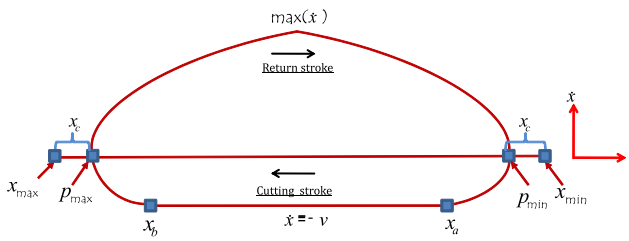

FIGURE 9. Phase diagram of the Whitworth mechanism at the output link.

where Θ is the cutting temperature average. It has to keep in mind that the cutting speed affects the life of the cutting tool and it is related with the heat generation.

There is a trade-off between increasing or decreasing the cutting speed. As the cutting speed gets higher, more heat is removed, which improves the performance in presence of friction. However, the temperature of the tool increases [37]. On the other hand, the reduction of the cutting speed increases the amount of the heat flowing to the workpiece. It rises the temperature of the workpiece [37], [38].

The proposed approach considers a constant cutting speed which balances the trade-off of the problem mentioned above. Uniform cuts are obtained throughout the workpiece and reduces dimensional errors. Furthermore, the machining temperature is approximately constant in the whole process.

VI. SIMULATION STUDIES

The Whitworth mechanism, shown in Figure 8 is analyzed with the approach mentioned above. There is a main difference between the slider dynamics of the Whitworth mechanism and the classical slider-crank mechanism (Figure 2). In the first case, the slider moves in the opposite direction, as it is shown in Figure 9. Hence, the cutting stroke has a negative sign, i.e., $z = -1$.

The slider dynamics [32] written as in (14) is

$$m_6\ddot{x} = u - \left(\sum_{i=1}^{n'} \rho_i^2(\boldsymbol{q}')\right)^{-1} \rho_x^2(\boldsymbol{q}')F_x \tag{35}$$

where m_6 is the slider mass, and $\rho_x(\boldsymbol{q}') = -\frac{r_2 r_4}{r_3}\cos(q - \theta_4)\sin(\theta_4 - \theta_5)\sec(\theta_5)$; here r_1, r_2, r_4, r_5 and r_7 stand to fixed lengths; r_3, θ_4, θ_5 and x are the secondary variables $\boldsymbol{s}$ of the generalized coordinates vector $\boldsymbol{q}'$.

The simulations were made with Matlab/Simulink®. The Runge Kutta 4th order method was used with a fixed step size of 1 ms. The mechanism kinematic parameters were chosen in such a way that the crank has full turn. The mechanism kinematics is given in the Appendix. The proposed kinematic parameters are $r_1 = 0.15$ m, $r_2 = 0.1$ m, $r_4 = 0.35$ m, $r_5 = 0.2$ m and $r_7 = 0.35$ m. The value of the proposed slider mass is $m_6 = 1$ kg.

A. SIMULATIONS USING DIFFERENT MATERIALS

The simulations evaluated workpieces made with five different materials. Their respective cutting speeds and contact forces were considered. The length of each workpiece was $L_d = 0.3$ m. The contact force between the workpiece and the slider was applied horizontally in the opposite direction of the slider movement. The magnitude of the force was defined in terms of the depth, cutting velocity and the material of the workpiece [39].

A threshold of $x_c = 0.0137$ m was proposed. The joint positions, where the Jacobian $\rho_x(\cdot)$ is equal to zero, were: $q_{\min} = -0.729728$ and $q_{\max} = -2.4119$ rad. Those joint positions were mapped to the task space singularity points through the mechanism forward kinematics (see Appendix) as: $x_{\min} = 0.05428$ m and $x_{\max} = -0.4124$ m. Hence, the length of the slider stroke was $L_c = 0.4667$ m. The switching points were $p_{\min} = 0.0406$ m and $p_{\max} = -0.3987$ m.

The parameters of the trapezoidal trajectory and the control gains of each workpiece are given in Table 1. Here t_0 stands to the initial time of the cutting stroke. The control gains were chosen in such a way that the contact force and the vanishing term $\lambda s(t_0)$ were compensated. The TBG gains were proposed as $\varepsilon = \delta = 0.001$.

The return stroke was divided into two parts. The first one considered a torque of $\tau = 8.65$ Nm. In the second part, a torque of $\tau = -8$ Nm was used. The speed response was smoothed in such a way that the return stroke trajectory converges smoothly to the switching point $p_{\min}$ by using the TBG attraction. After that, the cutting stroke starts again.

Figure 10 shows the speed control results for each material. The parameters of Table 1 were used. Each material has a characteristic cutting speed, which directly affects the duration of the cutting stroke. Figures 10(a), 10(d),10(g), 10(j) and 10(m) show the complete speed profile of the slider. It has to be observed that the duration of the cutting stroke increases for small cutting speeds, as it is shown in Figure 10(d). The return stroke trajectory was the same for all the materials,

TABLE 1. Trajectory parameters and Control Gains.

Material	v (m/s)	F_x (N)	t_c (s)	t_a (s)	x_a (m)	x_b (m)	t_b (s)	k_1	k_2	λ
Aluminum	-1.25	400	0.24	0.13	-0.0407	-0.3407	$t_0 + 0.104$	100	1	40
Steel	-0.25	80	1.2	0.67	-0.0432	-0.3432	$t_0 + 0.536$	30	1	10
Brass	-0.75	240	0.4	0.22	-0.0419	-0.3419	$t_0 + 0.176$	60	1	30
Titanium	-0.5	160	0.6	0.33	-0.0419	-0.3419	$t_0 + 0.264$	50	1	25
Bronze	-0.4	128	0.75	0.42	-0.0434	-0.3434	$t_0 + 0.336$	40	1	20

since it did not depend on the cutting speed. Notice that, the return stroke is faster than the cutting stroke since the mechanical advantage is exploited by using the joint space controller in open-loop.

There is a small overshoot due to the switching criterion and the TBG attraction at the end of the return stroke as it is shown in the phase diagrams. Figures 10(b), 10(e), 10(h), 10(k) and 10(n) show the tracking velocity error $\dot{e}$ of the cutting stroke. In these cases, there were two small overshoots. They were generated by the impacts between the slider and the workpiece at the points x_a and x_b, respectively. The second order SMC compensates the contact force and guarantees the constant speed profile throughout the workpiece. These impact overshoots can be reduced by increasing the gains k_1 or k_2. However, the switching criterion overshoot can be increased. So, there is a trade-off between the impact and the switching criterion overshoots. In other words, large control gains reduce the impact overshoots. However, the switching criterion overshoot is increased. Conversely, small control gains increase the impact overshoots and reduces the switching criterion overshoot.

Figures 10(c), 10(f), 10(i), 10(l) and 10(o) show the phase diagram of the slider dynamics. Here, the cutting stroke has a constant velocity profile in the interval $[x_a, x_b]$. Outside of this interval, the trajectory advances smoothly to the switching point $p_{\max}$, then the controller is switched into a constant torque that returns the mechanism trajectory to the next switching limit point $p_{\min}$ with the help of the TBG attraction. For small cutting speeds, the parabolic blends were almost linear, as it is shown in Figure 10(f). Hence, the transition from the task space controller to the constant torque and vice versa by the switching criterion, would present overshoots at the beginning and the end of the return stroke.

B. COMPARISONS

The performance of the hybrid joint-task space controller is compared with the reciprocating method using a joint space controller. The workpiece is not considered in this simulation in order to make more fair the performance comparison between these two controllers. The aluminum cutting velocity of Table 1 is used as desired cutting velocity. The simulation satisfies the aluminum parameters of Table 1 and the points of the trapezoidal profile of last section. The same control gains for the hybrid joint-task space controller were used.

The reciprocating method was designed in the graphic interface of Working Model® 2004. A constant joint velocity of $\dot{q}_d = 8.95$ rad/s was used to achieve an approximate linear velocity $\dot{x} \approx -1.25$ m/s (Aluminum cutting velocity, see Table 1) at the output link. Figure 11 exhibits the comparison results.

The results show that the reciprocating method needs an optimization procedure, that is, a mechanism synthesis to guarantee a constant cutting speed profile. Furthermore, different mechanism synthesis have to be done to take into account different range of cutting velocities which is a tedious procedure. Furthermore, the reciprocating method did not consider the workpiece since it assumes that at all times the crank velocity will be constant and therefore the slider velocity will also be approximately constant.

One advantage of the reciprocating method is that the singularities are avoided and the mechanical advantage is always satisfied due to the mechanism configuration. Notice that, the return stroke of the reciprocating method is faster than the hybrid controller due to the choice of constant torque T; this torque can be increased as large as the characteristics of the actuator allow. However, the hybrid controller does not need an optimization procedure to guarantee a constant cutting velocity, instead it takes into account the workpiece and the mechanism configuration for the cutting velocity profile design which is the major contribution of this work.

C. DISCUSSIONS

From the previous results, it was shown that the proposed method has accurate tracking results along the cutting stroke (see cutting stroke speed error $\dot{e}$ results). Since this kind of mechanisms has a linear movement at the output link, it is possible to simplify the non-linear dynamics of the complete mechanism. In this way, the slider dynamics, which is a linear system with a disturbance, can be used. The cutting stroke is controlled by the second-order SMC. It compensates the contact force when the mechanism touches the workpiece. Since the return stroke does not perform any operation, then it is not necessary to control it. The TBG forces the mechanism dynamics converge to the switching limit point $p_{\min}$. It helps the SMC to start at the sliding manifold. The switching points guarantee a full turn of the crank and avoid the singularity points.

The overshoots at the end of the return stroke can be seen as a jerk. A significant cumulative damage on the machine bearings and fatigue damage on machine parts are caused during their life time. Such jerks can be reduced by introducing some damping at the end of the return stroke or using a neural network [40]. Furthermore, the time delays and packet losses in the transmission of the information between the computer,

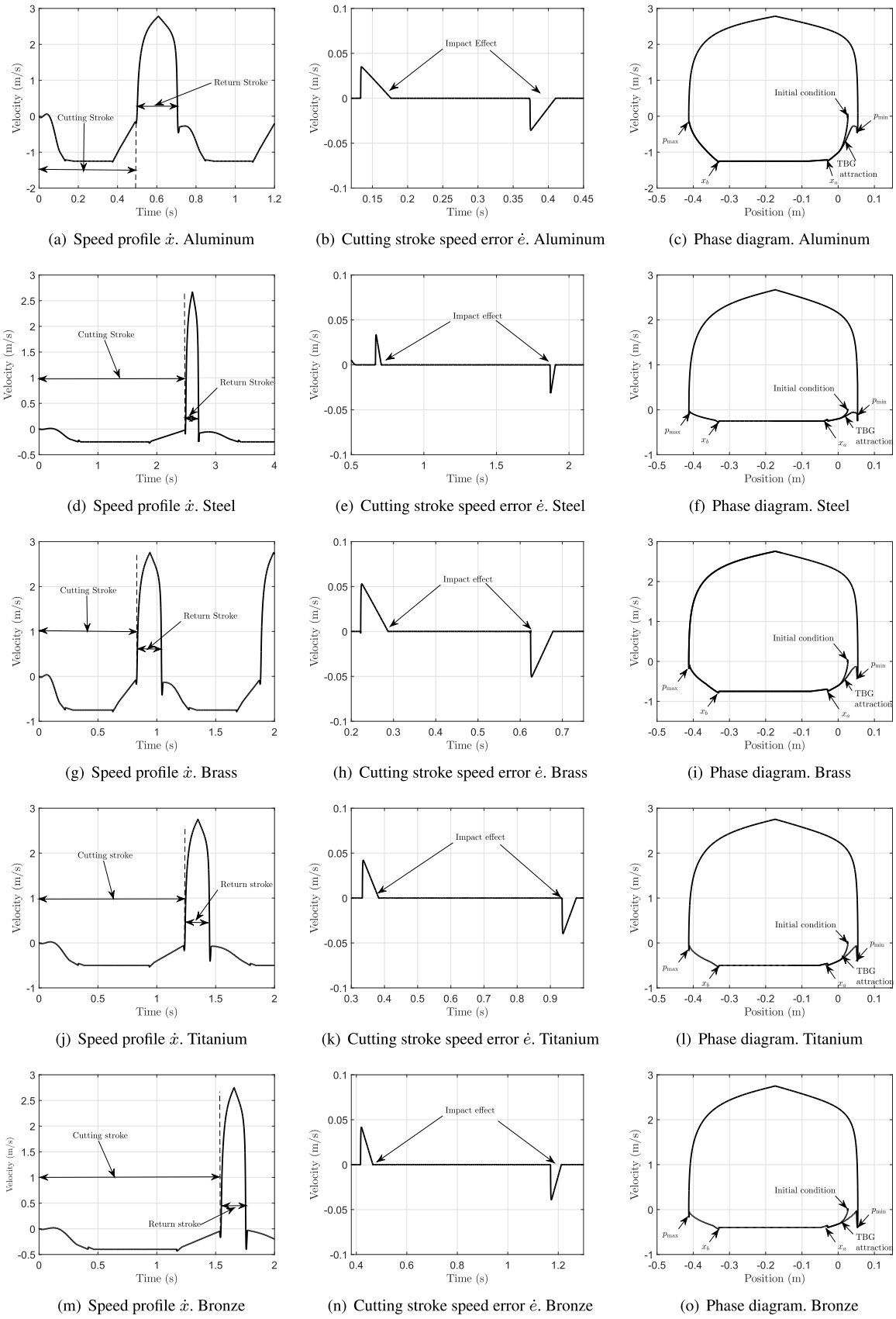

(a) Speed profile $\dot{x}$. Aluminum (b) Cutting stroke speed error $\dot{e}$. Aluminum (c) Phase diagram. Aluminum

(d) Speed profile $\dot{x}$. Steel (e) Cutting stroke speed error $\dot{e}$. Steel (f) Phase diagram. Steel

(g) Speed profile $\dot{x}$. Brass (h) Cutting stroke speed error $\dot{e}$. Brass (i) Phase diagram. Brass

(j) Speed profile $\dot{x}$. Titanium (k) Cutting stroke speed error $\dot{e}$. Titanium (l) Phase diagram. Titanium

(m) Speed profile $\dot{x}$. Bronze (n) Cutting stroke speed error $\dot{e}$. Bronze (o) Phase diagram. Bronze

FIGURE 10. Speed profile $\dot{x}$, Cutting stroke speed error $\dot{e}$, Phase diagram of each material under the parameters of Table 1.

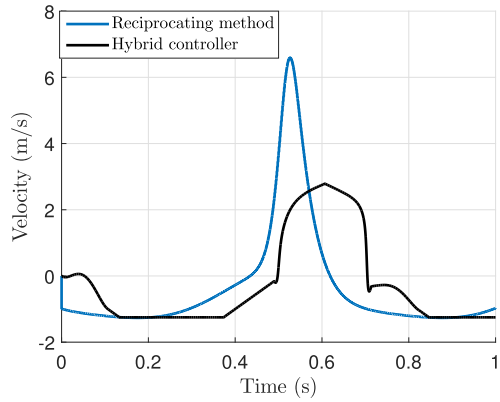

(a) Speed profile $\dot{x}$

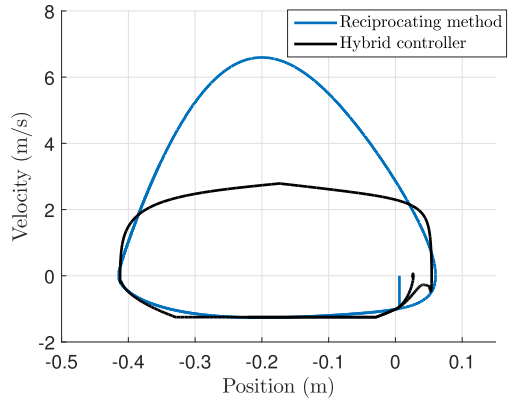

(b) Phase diagram comparisons

FIGURE 11. Comparison results between the reciprocating method and the hybrid joint-task space controller.

sensors and actuators must be taken into account in this kind of applications [41], [42]. These are topics in future research.

VII. CONCLUSION

In this paper, a constant speed control of slider-crank mechanisms for cutting process is presented. An hybrid joint-task space control law, which guarantees a constant cutting speed tracking, was considered. The mechanical advantage was considered and ensures full turn of the crank.

The cutting stroke was controlled by a task-space second-order SMC. In parallel, the return stroke was controlled in open-loop by a constant torque. The transitions between the task space controller and the constant torque was given by a switching criterion and a time-based generator. It avoids the singularity points and forces the system trajectories to converge to the switching point and sliding manifold in finite time. Stability of the second-order SMC is given using Lyapunov stability theory.

The speed profile was designed as a trapezoidal profile with parabolic blends. The workpiece and slider stroke lengths, the constant cutting speed and the singularity points were considered for the profile design.

Simulation studies were carried out to verify this approach using different cutting speeds and contact forces in accordance with the workpiece material. The results showed that the proposed approach holds for different cutting speeds and forces and can be extended for any slider-crank mechanism.

Future work addresses the jerk problem at the beginning and end of the return stroke, which is caused by the switching criterion.

APPENDIX. WHITWORTH KINEMATICS

The generalized variable for the Whitworth mechanism is q and the secondary variables are $\boldsymbol{s} = \begin{bmatrix}\theta_4 & \theta_5 & r_3 & x\end{bmatrix}^\top$. Its system of equations is

$$\begin{aligned} f_1(q,\boldsymbol{s}) &= r_3\cos(\theta_4) - r_2\cos(q) = 0 \\ f_2(q,\boldsymbol{s}) &= r_3\sin(\theta_4) - r_2\sin(q) - r_1 = 0 \\ f_3(q,\boldsymbol{s}) &= r_4\cos(\theta_4) + r_5\cos(\theta_5) - x = 0 \\ f_4(q,\boldsymbol{s}) &= r_4\sin(\theta_4) + r_5\sin(\theta_5) - r_7 = 0 \end{aligned} \tag{A.1}$$

The analytic solutions of (A.1) with respect to the secondary variables $\boldsymbol{s}$ are

$$\begin{aligned} \theta_4 &= \arctan\left(\frac{r_1 + r_2\sin(q)}{r_2\cos(q)}\right) \\ r_3 &= \frac{r_2\cos(q)}{\cos(\theta_4)} \\ \theta_5 &= \pi - \arcsin\left(\frac{r_7 - r_4\sin(\theta_4)}{r_5}\right) \\ x &= r_4\cos(\theta_4) + r_5\cos(\theta_5) \end{aligned} \tag{A.2}$$

The Jacobian $J(q)$ is obtained by differentiating (A.2)

$$J(q) = \begin{bmatrix} \frac{r_2\cos(q-\theta_4)}{r_3} \\ -\frac{r_2 r_4\cos(q-\theta_4)\cos(\theta_4)\sec(\theta_5)}{r_3 r_5} \\ -r_2\sin(q-\theta_4) \\ -\frac{r_2 r_4\cos(q-\theta_4)\sin(\theta_4-\theta_5)}{r_3\cos(\theta_5)} \end{bmatrix} \tag{A.3}$$

The Jacobian $\rho_x(q)$ is restricted by the system equations and the position of the slider as,

$$\rho_x(q) = -\frac{r_2 r_4\cos(q-\theta_4)\sin(\theta_5-\theta_4)}{r_3\cos(\theta_5)} \tag{A.4}$$

The extended generalized coordinates are

$$\begin{aligned} \boldsymbol{q}' &= \begin{bmatrix} q & r_3 & \theta_4 & \theta_5 & x \end{bmatrix}^\top \\ \dot{\boldsymbol{q}}' &= \begin{bmatrix} \dot{q} & \dot{r}_3 & \dot{\theta}_4 & \dot{\theta}_5 & \dot{x} \end{bmatrix}^\top \end{aligned} \tag{A.5}$$

The extended Jacobian $\boldsymbol{\rho}(\boldsymbol{q}')$ is

$$\begin{aligned} \dot{\boldsymbol{q}}' &= \boldsymbol{\rho}(\boldsymbol{q}')\dot{q} \\ \begin{bmatrix} \dot{q} \\ \dot{r}_3 \\ \dot{\theta}_4 \\ \dot{\theta}_5 \\ \dot{x} \end{bmatrix} &= \underbrace{\begin{bmatrix} 1 \\ -r_2\sin(q-\theta_4) \\ \frac{r_2\cos(q-\theta_4)}{r_3} \\ -\frac{r_2 r_4\cos(q-\theta_4)\cos(\theta_4)\sec(\theta_5)}{r_3 r_5} \\ -\frac{r_2 r_4\cos(q-\theta_4)\sin(\theta_4-\theta_5)}{r_3\cos(\theta_5)} \end{bmatrix}}_{\boldsymbol{\rho}(\boldsymbol{q}')} \dot{q} \end{aligned} \tag{A.6}$$

REFERENCES

[1] A. Perrusquia, J. A. Flores-Campos, and W. Yu, "Simple optimal tracking control for a class of closed-chain mechanisms in task space," in *Proc. 16th Int. Conf. Electr. Eng., Comput. Sci. Autom. Control (CCE)*, Sep. 2019, pp. 1–6.

[2] R. F. Fung, F. Lin, R. Wai, and P. Lu, "Fuzzy neural network control of a motor-quick-return servomechanism," *Mechatronics*, vol. 10, pp. 145–167, Feb./Mar. 2000.

[3] H.-S. Yan and W.-R. Chen, "A variable input speed approach for improving the output motion characteristics of watt-type presses," *Int. J. Mach. Tools Manuf.*, vol. 40, no. 5, pp. 675–690, Apr. 2000.

[4] C. Gosselin and J. Angeles, "Singularity analysis of closed-loop kinematic chains," *IEEE Trans. Robot. Autom.*, vol. 6, no. 3, pp. 281–290, Jun. 1990.

[5] A. Perrusquia, W. Yu, and X. Li, "Multi-agent reinforcement learning for redundant robot control in task-space," *Int. J. Mach. Learn. Cybern.*, vol. 12, pp. 231–241, Jul. 2020.

[6] P. Flores, "Modeling and simulation of wear in revolute clearance joints in multibody systems," *Mechanism Mach. Theory*, vol. 44, pp. 1211–1222, Jun. 2009.

[7] A. Perrusquía, W. Yu, A. Soria, and R. Lozano, "Stable admittance control without inverse kinematics," in *Proc. 20th IFAC World Congr.*, vol. 50, no. 1, 2017, pp. 15835–15840.

[8] R.-F. Fung and C.-F. Chang, "Force/motion sliding mode control of three typical mechanisms," *Asian J. Control*, vol. 11, no. 2, pp. 196–210, Mar. 2009.

[9] E. Zheng and X. Zhou, "Modeling and simulation of flexible slider-crank mechanism with clearance for a closed high speed press system," *Mechanism Mach. Theory*, vol. 74, pp. 10–30, Apr. 2014.

[10] J. Risso and A. Cardona, "Influencia De Las deformaciones En modelos Dinámicos De Trenes De engranajes," *Mecánica Computacional*, vol. XXVI, pp. 3056–3077, Oct. 2007.

[11] M. Mehdi Fateh and H. Farhangfard, "On the transforming of control space by manipulator Jacobian," *Int. J. Control, Automat., Syst.*, vol. 6, no. 1, pp. 101–108, Feb. 2008.

[12] A. Perrusquia, C. Tovar, A. Soria, and J. C. Martinez, "Robust controller for aircraft roll control system using data flight parameters," in *Proc. 13th Int. Conf. Electr. Eng., Comput. Sci. Autom. Control (CCE)*, Sep. 2016, pp. 1–5.

[13] F.-J. Lin and R.-J. Wai, "Adaptive and fuzzy neural network sliding-mode controllers for motor-quick-return servomechanism," *Mechatronics*, vol. 13, no. 5, pp. 477–506, Jun. 2003.

[14] A. Perrusquia, J. A. Flores-Campos, and C. R. Torres-San-Miguel, "A novel tuning method of PD with gravity compensation controller for robot manipulators," *IEEE Access*, vol. 8, pp. 114773–114783, 2020.

[15] V. Parra-Vega, S. Arimoto, Y.-H. Liu, G. Hirzinger, and P. Akella, "Dynamic sliding PID control for tracking of robot manipulators: Theory and experiments," *IEEE Trans. Robot. Autom.*, vol. 19, no. 6, pp. 967–976, Dec. 2003.

[16] J. A. Flores-Campos, J. A. Perrusquía Guzmán, J. A. Beltrán-Fernández, and L. H. Hernández-Gómez, "Sliding mode control of a water-displacement based mechanism applied to the orientation of a parabolic-trough solar concentrator," *Defect Diffusion Forum*, vol. 370, pp. 90–97, Jan. 2017.

[17] A. Perrusquia and W. Yu, "Task space human-robot interaction using angular velocity Jacobian," in *Proc. Int. Symp. Med. Robot. (ISMR)*, Apr. 2019, pp. 1–7.

[18] R. G. Rodríguez and P. Zegers, "Cartesian controllers for tracking of robot manipulators under parametric uncertainties," in *Proc. INTECH*, 2011, pp. 109–115. [Online]. Available: http://www.intechopen.com/books/robot-arms

[19] J. Nakanishi, R. Cory, M. Mistry, J. Peters, and S. Schaal, "Operational space control: A theoretical and empirical comparison," *Int. J. Robot. Res.*, vol. 27, no. 6, pp. 737–757, Jun. 2008.

[20] A. B. Abdullah, L. Y. Chia, and Z. Samad, "The effect of feed rate and cutting speed to surface roughness," *Asian J. Scientific Res.*, vol. 1, no. 1, pp. 12–21, Dec. 2007.

[21] F. X. Wu, W. J. Zhang, Q. Li, and P. R. Ouyang, "Integrated design and PD control of high-speed closed-loop mechanisms," *J. Dyn. Syst., Meas., Control*, vol. 124, no. 4, pp. 522–528, Dec. 2002.

[22] W. H. Hsieh and C. H. Tsai, "A study on a novel quick return mechanism," *Trans. Can. Soc. Mech. Eng.*, vol. 33, no. 3, pp. 487–500, 2009.

[23] R. F. Fung and K. W. Chen, "Constant speed control of the quick return mechanism driven by a DC motor," *JSME Int. J. C Mech. Syst., Mach. Elements Manuf.*, vol. 40, no. 3, pp. 454–461, 1997.

[24] J.-L. Ha, R.-F. Fung, K.-Y. Chen, and S.-C. Hsien, "Dynamic modeling and identification of a slider-crank mechanism," *J. Sound Vib.*, vol. 289, nos. 4–5, pp. 1019–1044, Feb. 2006.

[25] H.-S. Yan and G.-J. Yan, "Integrated control and mechanism design for the variable input-speed servo four-bar linkages," *Mechatronics*, vol. 19, no. 2, pp. 274–285, Mar. 2009.

[26] H.-S. Yan and W.-R. Chen, "On the output motion characteristics of variable input speed servo-controlled slider-crank mechanisms," *Mechanism Mach. Theory*, vol. 35, no. 4, pp. 541–561, Apr. 2000.

[27] A. Perrusquía and W. Yu, "Neural H_2 control using continuous-time reinforcement learning," *IEEE Trans. Cybern.*, early access, Nov. 24, 2020, doi: 10.1109/TCYB.2020.3028988.

[28] K. Vinu and A. Ghosal, "Singularity analysis of closed-loop mechanisms and parallel manipulators," in *Proc. 15th Nat. Conf. Mach. Mech.*, 2011, pp. 1–9.

[29] A. Perrusquia, W. Yu, and X. Li, "Redundant robot control using multi agent reinforcement learning," in *Proc. IEEE 16th Int. Conf. Autom. Sci. Eng. (CASE)*, Aug. 2020, pp. 1650–1655.

[30] J. A. Flores Campos and A. Perrusquía, "Slider position control for slider-crank mechanisms with jacobian compensator," *Proc. Inst. Mech. Eng., I, J. Syst. Control Eng.*, vol. 233, no. 10, pp. 1413–1421, Nov. 2019.

[31] F. Ghorbel, "Modeling and PD control of closed-chain mechanical systems," in *Proc. 34th IEEE Conf. Decis. Control*, New Orleans, LA, USA, Dec. 1995, pp. 540–542.

[32] A. Perrusquia, J. A. Flores-Campos, C. R. Torres-Sanmiguel, and N. Gonzalez, "Task space position control of slider-crank mechanisms using simple tuning techniques without linearization methods," *IEEE Access*, vol. 8, pp. 58435–58442, 2020.

[33] O. D. Ramirez, V. P. Vega, M. D. Montiel, M. P. Cardenas, and R. H. Gomez, "Cartesian sliding PD control of robot manipulator for tracking in finite time: Theory and experiments," in *DAAAM International Scientific Book*. Vienna, Austria: DAAAM International Vienna, 2008, pp. 257–272.

[34] A. Perrusquía and W. Yu, "Human-in-the-loop control using euler angles," *J. Intell. Robotic Syst.*, vol. 97, pp. 271–285, Jul. 2019.

[35] A. Kus, Y. Isik, M. Cakir, S. Coşkun, and K. Özdemir, "Thermocouple and infrared sensor-based measurement of temperature distribution in metal cutting," *Sensors*, vol. 15, no. 1, pp. 1274–1291, Jan. 2015.

[36] E. Lowen and M. C. Shaw, "On the analysis of cutting tool temperatures," *Trans. ASME*, vol. 76, pp. 217–231, Mar. 1954.

[37] S. Yujing, S. Jie, L. Jianfeng, and X. Qingchun, "An experimental investigation of the influence of cutting parameters on cutting temperature in milling Ti6Al4V by applying semi-artificial thermocouple," *Int. J. Adv. Manuf. Technol.*, vol. 70, pp. 765–773, Sep. 2014.

[38] A. Fata, "Temperature measurement durinf machining depending on cutting conditions," *P & A Sci. Technol.*, vol. 1, pp. 16–21, Jun. 2011.

[39] S. L. Gombi and D. S. Ramakrishna, "Estimation of impact effect on the cutting tool of a shaper from measurement of responses during machining," *J. Manuf. Sci. Prod.*, vol. 12, nos. 3–4, pp. 161–169, Jan. 2012.

[40] A. Perrusquía and W. Yu, "Discrete-time H_2 neural control using reinforcement learning," *IEEE Trans. Neural Netw. Learn. Syst.*, early access, Oct. 5, 2020, doi: 10.1109/TNNLS.2020.3026010.

[41] Z. Gu, P. Shi, D. Yue, S. Yan, and X. Xie, "Memory-based continuous event-triggered control for networked T-S fuzzy systems against cyber-attacks," *IEEE Trans. Fuzzy Syst.*, early access, Jul. 29, 2020, doi: 10.1109/TFUZZ.2020.3012771.

[42] Z. Gu, J. H. Park, D. Yue, Z.-G. Wu, and X. Xie, "Event-triggered security output feedback control for networked interconnected systems subject to cyber-attacks," *IEEE Trans. Syst., Man, Cybern. Syst.*, early access, Jan. 7, 2020, doi: 10.1109/TSMC.2019.2960115.

JUAN ALEJANDRO FLORES-CAMPOS (Member, IEEE) received the M.Sc. degree in mechanical engineering from UNAM, Mexico, and the Ph.D. degree in mechanical engineering from the National Polytechnic Institute, in 2006. He is currently a Lecturer with the Interdisciplinary Professional Unit in Engineering and Advanced Technologies, National Polytechnic Institute (UPIITA-IPN). His research interests include dynamic modeling, closed-loop mechanisms control, nonlinear control, and renewable energy.

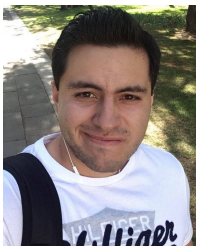

ADOLFO PERRUSQUÍA (Member, IEEE) received the B.Eng. degree in mechatronic engineering from the Interdisciplinary Professional Unit in Engineering and Advanced Technologies, National Polytechnic Institute (UPIITA-IPN), in 2014, and the M.Sc. and Ph.D. degrees in automatic control from the Department of Automatic Control, Center for Research and Advanced Studies, National Polytechnic Institute (CINVESTAV-IPN), in 2016 and 2020, respectively. He is currently a Research Fellow with Cranfield University. His research interests include robotics, mechanisms, machine learning, reinforcement learning, nonlinear control, system modeling, and system identification. He is a member of the IEEE Computational Intelligence Society.

LUIS HÉCTOR HERNÁNDEZ-GÓMEZ received the D.Phil. degree from Oxford University. He is currently a Lecturer with the Higher School of Mechanical and Electrical Engineering, National Polytechnic Institute. His research interests include stress analysis, biomechanics, numerical methods, and nuclear safety. He is a member of ASME and the Mexican Academy of Science.

NOÉ GONZÁLEZ received the M.Sc. degree in mechanical engineering from National Polytechnic Institute, in 2016, where he is currently involved in a research project with the objective to get a Doctor in Science degree. His research interest includes control, mechanisms, modeling, and simulation of robotic systems and vision.

ALEJANDRA ARMENTA-MOLINA received the M.Sc. degree from National Polytechnic Institute, in 2014, where she is currently conducting research to obtain her Doctorate in Sciences degree. Her research interest includes electronics, control, and numerical simulation.